NASA-TM-81451 19800012848

NASA Technical Memorandum 81451

STEADY-STATE PERFORMANCE OF A J85-21 COMPRESSOR AT 100 PERCENT OF DESIGN SPEED WITH AND WITHOUT INTERSTAGE RAKE BLOCKAGE

Roger A. Werner
Lewis Research Center
Cleveland, Ohio

March 1980

STEADY-STATE PERFORMANCE OF A J85-21 COMPRESSOR AT 100 PERCENT OF DESIGN SPEED WITH AND WITHOUT INTERSTAGE RAKE BLOCKAGE

Roger A. Werner

National Aeronautics and Space Administration
Lewis Research Center
Cleveland, Ohio 44135

SUMMARY

Steady-state J85-21 measurements at 100 percent of design speed are presented to determine compressor performance with blockage resulting from various instrumentation configurations. The configurations consisted of 4 or 12 inlet rakes; 12 or 24 instrumented vanes for stages 1 to 3; and 0, 12, or 24 interstage rakes for stages 4 to 9. This instrumentation generated individual flow-passage blockages of 2.5 to 4.5 percent for the instrumented-vane passages and 12 to 22 percent for the interstage-rake passages.

At an inlet Reynolds number index of 1.0, compressor total-pressure ratio (8.30), airflow (24.05 kg/sec), compressor stage static-pressure-rise coefficients, turbine exit temperature (1000 K), and fuel flow (448 g/sec) remained constant during the rake comparisons. Compressor efficiency and compressor exit profiles were unchanged during inlet-rake and instrumented-vane comparisons. Efficiency dropped 0.3 percentage point from 81.6 percent when 12 or 24 interstage rakes were installed. However, this efficiency drop was within the observed data scatter. The profiles, although unaffected when 12 interstage rakes were used, became distorted upon insertion of 24 interstage rakes.

Compressor exit profiles also remained unchanged at 1.69- and 1.95-inlet-RNI conditions with changes of inlet rakes, changes of instrumented vanes, and 0 or 12 interstage rakes.

INTRODUCTION

J85-21 compressor performance corresponding to steady-state engine operation at 100 percent of design speed was investigated to determine internal instrumentation blockage effects. Performance deterioration caused by instrumentation blockage has always been a concern in airbreathing engine research (refs. 1 and 2). Currently very little published information can be found that deals with this problem.

A joint Air Force - NASA full-scale engine research program was conducted at the Lewis Research Center on the J85-21 turbojet engine. This program primarily consisted of two phases: internal compressor aerodynamics, and compressor aeromechanical instability (flutter). Both phases used internal compressor instrumentation comprised of removable interstage rakes - which were similar to those employed in a previous aerodynamics investigation (ref. 3) - and instrumented vanes. A portion of the aero-

dynamics phase compared compressor performances with different instrumentation configurations to determine the blockage effects. If the performance changed significantly, the internal compressor measurements may not represent normal J85-21 operation. This report is the initial report for the aerodynamics phase; part of the aeromechanical investigation has already been published in references 4 and 5. Technical assistance on the test plan and compressor instrumentation was provided by the engine manufacturer, General Electric Co.

In this investigation the effects of probe blockage on compressor performance were determined from comparisons of steady-state engine test data at similar test conditions but with different instrumentation configurations. These data included compressor pressure ratio, compressor efficiency, airflow, rotor speed, turbine exit temperature, fuel flow, exhaust nozzle position, compressor stage static-pressure-rise coefficients, and compressor exit profiles (pressure and temperature) for a Reynolds number index (RNI) of 1.0, where RNI = $\delta/(\phi \sqrt{\theta})$. In addition, compressor exit profiles for inlet RNI of 1.69 and 1.95 are presented.

APPARATUS AND PROCEDURE

Engine

The J85-21 is a lightweight, single-spool turbojet engine with a rated nonafterburning thrust of 15.5 kN (3500 lbf). The engine has a nine-stage axial compressor with variable inlet guide vanes and variable stators for the first three stages. It has an annular combustor, a two-stage axial-turbine, an afterburner (not used), and a variable-area exhaust nozzle. The engine used in this program, serial number 225326, was received from the Air Force with 6.3 hours engine time in an F-5 aircraft. In 1975, this engine was updated to production standards with modifications that included the reblading of compressor rotor stages 4 and 6. The first-stage turbine diaphragm, however, has a slightly smaller area than those in production engines.

Early in the test program the engine had to be disassembled to repair turbine damage sustained when an interstage rake failed on compressor stage 9. Midway into the aerodynamics program a compressor stall investigation was conducted during which 79 stalls were experienced by the engine. (A reduced-area turbine diaphragm was used.) After the stall investigation the program continued with some additional comparison measurements with and without interstage rakes. Upon program completion a crack was discovered in the compressor and mainframe cases, including the mating flanges.

Results from testing with this engine have been reported by NASA in references 4 to 6.

Installation

The engine was installed in an altitude test chamber as shown in figure 1. The installation was a conventional direct connection with a bellmouth located in an inlet plenum upstream of the engine altitude chamber

(fig. 2). The altitude chamber included a forward bulkhead separating the chamber from the inlet plenum. Conditioned air was supplied to the plenum at the desired pressure and temperature. Engine exhaust products and altitude chamber cooling air passed into an exhaust collector that extended through a rear bulkhead. The altitude chamber pressure was controlled by values downstream of the exhaust collector. Jet-A1 fuel was used.

Instrumentation

Figures 2 and 3 give the pressure and temperature measurement locations. In addition to these locations there was a second set of static-pressure taps near 90° on the interior of the compressor case. These taps were not included in figure 3 because they were located on the lower compressor case.

The pressure measurements were obtained with the DAMPR system (ref. 7), except for measurements from station 3 and compressor stages 6 to 9, which were obtained with a Scanivalve system. The temperature measurements were taken with Chromel-Alumel thermocouples referenced to 339 K ovens. Temperature measurements included recovery corrections similar to those in reference 8. The turbine exit temperature T_5 was obtained with the production-engine thermocouple harness. (All symbols are defined in appendix A.)

The airflow calculation consisted of pressures from station 1 and temperatures from station 2. This calculation assumed uniform static pressure across the duct and uniform total pressure throughout the free stream. To check the validity of these assumptions, profile measurements were obtained in a separate investigation and are presented in appendix B.

Internal compressor flow blockage was produced by 12 or 24 instrumented vanes and 12 or 24 interstage rakes (fig. 3). The instrumented vanes, one of which is shown in figure 4, were used in the first three compressor stages. Removable interstage rakes, shown in figure 5, were used in the remaining compressor stages.

A cross section of a typical stator passage with an interstage rake and the passage width used for blockage determination are shown in figure 6. Average blockage, as computed at points along the entire radial penetration of a rake into a passage, and the blockage range (smallest and largest values computed) are presented in table I for the affected stator passages. The uncertainty of the blockage values was ±1 percent blockage.

Finally, the position of the variable-area exhaust nozzle is represented by NPI (nozzle position indicator). The NPI was determined with a linear potentiometer that measured the stroke between the hydraulic actuators and the exhaust nozzle unison ring.

Procedure

Test data are presented at 1.0-, 1.69-, and 1.95-inlet-RNI conditions. The primary condition, 1.0 RNI, represents sea-level static status for the engine inlet. Reynolds number index tolerances are ±0.01 for 1.0 RNI and ±0.02 for the two other conditions. The RNI conditions were obtained with

the following inlet pressure and temperature levels: 101 kPa (14.7 psia) and 287 to 293 K (517° to 527° R) for 1.0 RNI, 138 kPa (20 psia) and 292 K (525° R) for 1.69 RNI, and 200 kPa (29 psia) and 244 K (440° R) for 1.95 RNI. Test-cell altitude pressure was adjusted to hold the inlet-to-altitude ram pressure ratio greater than 1.1 for 1.0 RNI and greater than 2.9 for 1.69 and 1.95 RNI. In addition, corrected rotor speed was maintained between 99.75 and 100.20 percent of design speed.

Testing began with 24 instrumented vanes, and comparison data were recorded for 12 inlet rakes with and without 24 interstage rakes and for 4 inlet rakes with and without 12 interstage rakes. Then, after the number of instrumented vanes was reduced to 12, comparison data were taken for 4 inlet rakes with and without the 12 interstage rakes. These are the instrumentation configurations used for the analysis of blockage effects.

Exhaust nozzle position was scheduled by afterburner fuel control for testing with 24 instrumented vanes and, because of fuel control instabilities, by manual control for testing with 12 instrumented vanes. To insure the proper nozzle position at various throttle angles, full-travel calibrations of these parameters were performed before each test run.

RESULTS AND DISCUSSION

The first section compares overall compressor pressure ratio, efficiency, airflow, and speed as functions of nozzle position indicator (NPI) for the six combinations of inlet, vane, and interstage instrumentation. The test conditions were 1.0 inlet RNI and 100 percent rotor speed. Additionally, turbine exit temperature and fuel flow are presented as a check for blockage effects that may not have been detected by the compressor measurements. Performance was corrected to engine inlet conditions in order to minimize changes caused by variations of inlet pressure and temperature about the desired levels. Performance at zero NPI is summarized in table II.

The remaining sections continue to investigate blockage effects by comparing compressor exit profiles at 1.0, 1.69, and 1.95 RNI and compressor stage static-pressure-rise coefficients at 1.0 RNI for the instrumentation configurations.

Overall Compressor Performance at 1.0 RNI

Total-pressure ratio. - Figure 7(a) shows that the overall compressor total-pressure ratio decreased from approximately 8.30 as NPI increased from zero. (Zero NPI corresponds to a fully closed nozzle with NPI increasing as the nozzle opens.) Inspection of the data does not correlate this pressure ratio decrease with changes of inlet, vane, or interstage instrumentation. The pressure ratio decrease was then probably a consequence of the NPI change.

The NPI level for the 24-instrumented-vane data was positioned by the engine control system. As discussed later, in the section on turbine exit temperature T_5, NPI values greater than zero are not the result of the engine control's T_5-control function. The nonzero NPI values were most likely associated with the history of problems experienced by the particular

control and actuating units on the engine during the program. Nonzero NPI values obtained while the engine was on manual control for the 12-instrumented-vane data were a result of insufficient facility hydraulic pressure to close the nozzle.

The systematic uncertainty (bias error) of pressure ratio was estimated to be less than 0.02. The uncertainty was computed by combining the estimated bias of the two measurement systems (DAMPR and Scanivalve) and using a weighted root-sum-square error equation. This equation is given in appendix C. Furthermore a random pressure ratio variation of less than 0.02 was determined from the data scatter along the line indicated in figure 7(a). This variation can be caused by drifting of the engine and test chamber conditions as well as by the data measurement systems.

Although the NPI measurement system was calibrated for accurate on-line monitoring of the nozzle schedule, similar attention was not provided to the data recording system. (During this program, NPI measurements for data analysis were not anticipated.) Therefore percent NPI values were derived from calibrations based on hand-logged readings and have uncertainties estimated to be at least 0.3 percent. Random NPI variation (data scatter), determined when there was no throttle movement, was also 0.3 percent. The pressure ratio at zero NPI, its systematic uncertainty and random data scatter, and the NPI uncertainty and data scatter are listed in table II.

Efficiency. - Compressor adiabatic efficiency is shown in figure 7(b) for six instrumentation configurations. Two efficiency levels are indicated: one without interstage rakes (81.6 percent), and a 0.3 percentage point lower efficiency with interstage rakes (81.3 percent). However, the 0.3-percentage-point drop is nearly equal to the ±0.4-percentage-point data scatter for each level. Furthermore each efficiency level remained constant with changes of NPI and with changes of inlet rakes and instrumented vanes.

The efficiency computation was based on the air composition and thermodynamic properties given in reference 9. Ignoring any errors inherent in this source, we determined the systematic uncertainty of efficiency resulting from measurement system bias (appendix C) to be ±0.6 percent. Efficiency values, along with their systematic uncertainty and observed data scatter, are presented in table II.

Corrected airflow and rotor speed. - As shown in figure 8(a) the corrected airflow remained constant at 24.05 kg/sec (53.0 lbm/sec) with changes of NPI and instrumentation configuration. The combination of measurement uncertainties resulted in an airflow systematic uncertainty of 0.15 kg/sec (0.3 lbm/sec) with an observed data scatter limit of the same value. The corrected rotor speed (fig. 8(b)) was set within 0.25 percent of the desired 100 percent value, with an uncertainty measurement of 0.1 percent.

Corrected turbine exit temperature and fuel flow. - By decreasing with increasing NPI, the turbine exit temperature and fuel flow measurements (fig. 9) supported the inverse relationship between compressor pressure ratio and NPI (fig. 7(a)). Since both turbine exit temperature and fuel flow exhibited fairly large data scatter, only dashed lines were used to represent the trends on the figure. These two measurements apparently were not influenced by instrumentation effects such as that of interstage rakes lowering the compressor efficiency in figure 7(b).

Even so, it is interesting to note a possible relationship between these measurements and efficiency for two sets of instrumentation configura-

tions. First, the 4-24-0 (inlet-vane-interstage) probe configuration has values below the dashed lines in figure 9 and has a relatively high efficiency (81.9 percent) in figure 7(b). Second, the 4-12-0 probe configuration has values slightly above the dashed lines in figure 9 and has a low efficiency (81.3 percent) in figure 7(b). For these points the increase or decrease in efficiency is seemingly reflected by a change in temperature and fuel flow in the opposite direction. The causes of these possible changes are unknown at this time.

The solid symbols in figure 9(a) represent temperature-limit operation of the turbine. The limit occurred for the solid 12-24-0 data as a consequence of a higher engine inlet air temperature of 292 K for this test condition as compared with 287 to 290 K for the others. The solid 4-12-0 points, however, are at the limit for an inlet temperature of only 288 K. One possible explanation of nonzero NPI for the engine control of nozzle position points would be the operation of a protection system that increased NPI to keep the turbine exit temperature from exceeding the limit. But this could not have happened since most of the nonzero NPI points in figure 9(a) are not at the limit (open symbols).

For engine operation at zero NPI, figure 9 shows the corrected turbine exit temperature to have been about 1000 K (1800° R) and the corrected Jet-A1 fuel flow to have been about 448 g/sec (3560 lbm/hr). Respective systematic uncertainties were 4 kelvins (7 deg R) and 2 g/sec (15 lbm/hr), and data scatter limits at zero NPI were 4 kelvins (7 deg R) and 4 g/sec (30 lbm/hr).

Compressor Exit Profiles at 1.0 RNI

Compressor exit radial profiles for total pressure and temperature are shown in figures 10 and 11. The profiles are presented at each of the four rake locations for the six combinations of inlet, vane, and interstage instrumentation. Each point in the figure is an average of the data readings obtained for each configuration and is normalized by the face-averaged value. Although the profiles changed from rake to rake, at each rake the profiles were unaffected by changes of instrumentation other than operation with 24 interstage rakes. With 24 interstage rakes the increased blockage raised the relative temperature level at the 330° location and also distorted the pressure profile at 330° (fig. 10). Reviewing figure 3 shows that the 330° rake was in a good location to pick up the wakes of the interstage rakes but that the 30° rake was not. Data points that were invalid because of pressure measurement tube leaks and open thermocouples were omitted. Substitutions for the invalid data points, based on the profile information, were included in the face-averaged calculations.

Circumferential distribution of total pressure and temperature is shown in figures 12 and 13. The points are rake averages normalized with the face average. (Substitutions for invalid data are included.) Although the pressure distribution remained unchanged for the comparisons, the temperature profile became more pronounced for the 24 interstage rakes - especially at the 330° location, which is behind the left-side internal instrumentation. Additional circumferential rake locations at the compressor exit are required to pick up the right-side instrumentation effects and possibly the 12-interstage-rake instrumentation effects.

Static-Pressure-Rise Coefficients at 1.0 RNI

The compressor stage static-pressure-rise coefficients for each of the instrumentation configurations are compared in figures 14 and 15. The rise coefficients are an average of the right- and left-side measurements, and each point is an average of the readings taken for a given instrumentation configuration. The coefficient values were for the most part uninfluenced by instrumentation changes. The greatest variation occurred at stage 4, where the 24-instrumented-vane points are slightly (about 0.015) below the 12-instrumented-vane points.

Because of bad data, coefficient values could not be compared for instrumented-vane effects on the first three stages. To do this, interstage (stator inlet to stator inlet) static-pressure-rise coefficients were compiled and are presented in figures 16 and 17. Here the 24-instrumented-vane points are again slightly (0.01) below the 12-instrumented-vane data at stage 4. Also, the 12-inlet-rake points are slightly (0.02) below the 4-inlet-rake data at stage 3, and the 24-interstage-rake point is slightly (0.025) above the other data at stage 6.

Because common errors will cancel out in a ratio calculation, the systematic uncertainties of the rise coefficients resulting from the measurement system bias were essentially zero except at stage 5. At stage 5, systematic uncertainty of the rise coefficients could go up to ± 0.013 because of independent errors from the two measurement systems (DAMPR and Scanivalve). Another source of error was the effect of static-pressure-tap geometry (ref. 10). This was a concern mainly for the larger diameter interstage pressure taps (figs. 16 and 17) and resulted in a maximum correction of 0.003.

Figure 18 compares right- and left-side variation and reading-to-reading variation for the stage static-pressure rise (instrumentation fixed). Comparing this figure with figures 14 and 15 shows that these variations were greater than those that might result from instrumentation changes.

Compressor Exit Profiles at 1.69 and 1.95 RNI

Instrumentation configuration comparisons are included for these two RNI because of the absence of previous experience (ref. 3) in aerodynamic testing above 100-kPa (1-atm) inlet pressure with interstage rakes installed. The compressor exit profiles (figs. 19 to 22) are used because these were the performance measurements most responsive to 24-interstage-rake effects (figs. 10 and 12). Each point in figures 19 to 22 is an average of two or more readings. Three sets of instrumentation configurations are compared in these figures without the appearance of inlet, vane, or interstage (12) instrumentation effects. Some pressure variations occurred in the tip regions of the radial profiles (figs. 19 and 20) and between 330° and 30° on the circumferential profiles (figs. 21 and 22), but these were no more than those that appeared in previous profiles (figs. 10 to 13).

SUMMARY OF RESULTS

Steady-state J85-21 engine measurements at 100 percent of design speed are presented to investigate the effects of various compressor instrumentation configurations on compressor performance. The instrumentation configurations consist of 4 or 12 inlet rakes; 12 or 24 instrumented vanes for stages 1 to 3; and 0, 12, or 24 interstage rakes for stages 4 to 9. This instrumentation produced individual stator-passage blockages of 2.5 to 4.5 percent for the instrumented vanes and 12 to 22 percent for the interstage rakes. Principal results of the investigation at 1.0-RNI (Reynolds number index) inlet conditions and at 1.69- and 1.95-RNI inlet conditions, where indicated, were as follows:

1. Instrumentation changes did not affect the compressor total-pressure ratio of 8.30, the airflow of 24.05 kg/sec (53.0 lbm/sec), the turbine exit temperature of 1000 K (1800° R), and the Jet-A1 fuel flow of 448 g/sec (3560 lbm/hr).

2. The compressor efficiency was 81.6 percent without interstage rakes installed and 81.3 percent with the rakes; the data scatter for both values was 0.4 percent. Efficiency was unaffected by the other instrumentation changes.

3. The compressor exit profiles were unchanged with instrumentation changes except when 24 interstage rakes were used; the profiles become distorted with 24 interstage rakes.

4. The stage and interstage static-pressure-rise coefficients were unchanged with instrumentation changes except for possibly very slight effects at one station or another.

5. At 1.69 and 1.95 RNI the compressor exit profiles remained unchanged with instrumentation changes. (Twenty-four interstage rakes were not used.)

APPENDIX A

SYMBOLS

D	duct diameter
h	isentropic enthalpy
M	Mach number
N	engine rotor speed, percent of design
P	total pressure, kPa (psia)
P_d	pressure differential between total and static
P_s	static pressure, kPa (psia)
ΔP_s	static-pressure rise, kPa (psia)
T	total temperature, K (^oR)
w_a	engine airflow, kg/sec (lbm/sec)
w_f	engine fuel flow, g/sec (lbm/hr)
δ	ratio of total pressure to standard sea-level static pressure
γ	specific-heat ratio
ϵ	bias error or systematic uncertainty
η_c	compressor adiabatic efficiency, ratio of isentropic enthalpy rise to actual enthalpy rise, percent
θ	ratio of total temperature to standard sea-level static temperature
ϕ	ratio of coefficient of viscosity to standard sea-level static coefficient of viscosity

Subscripts:

act	actual
av	average
i	individual probe
in	inlet to stage or interstage
interstage	stator inlet to stator inlet
is	isentropic
rake	rake-averaged value
s	static condition
stage	rotor inlet to rotor inlet
1	airflow measuring station
2	engine inlet
3	compressor exit
5	turbine exit
10	nozzle exit, external or altitude chamber condition

APPENDIX B

AIRFLOW-STATION PRESSURE PROFILES

Engine airflow was obtained through a radial summation of the boundary layer and free-stream flows at the airflow station (station 1). For this method assumptions of uniform static pressure across the duct and uniform total pressure throughout the free stream were used. These assumptions were experimentally investigated for their validity. Static-pressure and total-pressure profile measurements were acquired with four three-element pitot-static rakes. The rakes contained methyl-alcohol-filled U-tube manometers that provided differentials between rake probe and wall tap static pressures and between rake probe and boundary-layer tip probe total pressures. Pitot-static probe design and pressure corrections were taken from references 10 to 12. The inlet duct configuration was the same as for the engine tests but without the engine.

Figure 23 presents the pressure profiles at four inlet-RNI conditions, with each point representing an average of measurements from four rakes or four wall taps. This figure shows that the static pressure varied from 0.08 percent below the face average to 0.09 percent above but that the total pressure varied only ±0.03 percent about the average. With regard to airflow uncertainty at 1.0 RNI, the figure shows that using wall taps for static-pressure measurement resulted in an error of 0.05 percent and that using engine-test total-pressure probes (fig. 2) - which obtain measurements at the 45-percent area location - resulted in an error of 0.01 percent. Both these errors are smaller than the uncertainty (±0.15 percent) of the pressure data system used for the engine tests. Using engine-test instrumentation, combined with the uniformity assumptions, resulted in an airflow that was 0.11 percent low for the engine tests. This compares favorably with the ±0.6 percent error (±0.15 kg/sec) shown on table II in the report.

APPENDIX C

UNCERTAINTY EQUATIONS

Systematic uncertainties of the computed results were found by combining the bias errors of the measurement systems through weighted root-sum-square uncertainty equations. As presented in references 13 and 14 these uncertainty equations were derived from total differentials of the equations used for parameter calculation. These same uncertainty equations can also be derived by a Taylor's series expansion method, as given in reference 15. In keeping with reference 16 only independent errors were combined by this technique; common errors were allowed to cancel or to reinforce with each other as dictated in the derivation of the equation.

The following equations were used to compute the systematic uncertainties given in table II of the report:

Compressor total-pressure ratio:

$$\varepsilon_{P_3/P_2} = \frac{P_3}{P_2}\left[\left(\frac{\varepsilon_{P_2}}{P_2}\right)^2 + \left(\frac{\varepsilon_{P_3}}{P_3}\right)^2\right]^{1/2} \tag{C1}$$

where ε represents bias error or systematic uncertainty.

Compressor efficiency:

$$\varepsilon_{\eta_c} = \eta_c\left\{\left(\frac{100}{\eta_c}\frac{\partial h_{3,is}}{\partial T_2} - \frac{100-\eta_c}{\eta_c}\frac{\partial h_2}{\partial T_2}\right)^2\left(\frac{\varepsilon_{T_2}}{\Delta h_{act}}\right)^2 + \left(\frac{\partial h_3}{\partial T_3}\right)^2\left(\frac{\varepsilon_{T_3}}{\Delta h_{act}}\right)^2 + \left[\frac{100}{\eta_c}\frac{\partial h_{3,is}}{\partial (P_3/P_2)}\right]^2\left(\frac{\varepsilon_{P_3/P_2}}{\Delta h_{act}}\right)^2\right\}^{1/2} \tag{C2}$$

or

$$\varepsilon_{\eta_c} = \eta_c\left[\left(\frac{T_3/T_2}{\frac{T_3}{T_2}-1}\right)^2\left(\frac{\varepsilon_{T_2}}{T_2}\right)^2 + \left(\frac{T_3/T_2}{\frac{T_3}{T_2}-1}\right)^2\left(\frac{\varepsilon_{T_3}}{T_3}\right)^2 + \left(\frac{\gamma-1}{\gamma}\frac{\eta_c+100}{\eta_c}\right)^2\left(\frac{\varepsilon_{P_3/P_2}}{P_3/P_2}\right)^2\right]^{1/2} \tag{C3}$$

where h is the total enthalpy, $h_{3,is}$ is the isentropic enthalpy at station 3, and Δh_{act} is the actual enthalpy rise for the compressor $(h_3 - h_2)$.

Corrected airflow:

$$\varepsilon_{w_a\sqrt{\theta_2}/\delta_2} = \frac{w_a\sqrt{\theta_2}}{\delta_2}\left[4\left(\frac{\varepsilon_{D_1}}{D_1}\right)^2 + \alpha^2\left(\frac{\varepsilon_{P_1}}{P_1}\right)^2 + \alpha^2\left(\frac{\varepsilon_{P_{d,1}}}{P_{d,1}}\right)^2 + \left(\frac{P_1}{P_2}\right)^2\left(\frac{\varepsilon_{P_1}}{P_1} - \frac{\varepsilon_{P_2}}{P_2}\right)^2\right]^{1/2} \tag{C4}$$

with

$$\alpha = \left(\frac{P_1}{P_{s_1}} - 1\right)\left[\frac{\frac{\gamma_1 - 1}{2\gamma_1}}{\left(\frac{P_1}{P_{s,1}}\right)^{(\gamma_1-1)/\gamma_1} - 1} - 1\right] \tag{C5}$$

where D is the duct diameter, P_d is the pressure differential between total and static, and γ is the specific-heat ratio.

Corrected speed:

$$\varepsilon_{N/\sqrt{\theta_2}} = \frac{N}{\sqrt{\theta_2}}\left[\left(\frac{\varepsilon_N}{N}\right)^2 + \frac{1}{4}\left(\frac{\varepsilon_{T_2}}{T_2}\right)^2\right]^{1/2} \tag{C6}$$

Corrected turbine exit temperature:

$$\varepsilon_{T_5/\theta_2} = \frac{T_5}{\theta_2}\left[\left(\frac{\varepsilon_{T_5}}{T_5}\right)^2 + \left(\frac{\varepsilon_{T_2}}{T_2}\right)^2\right]^{1/2} \tag{C7}$$

Corrected fuel flow:

$$\varepsilon_{w_f/\delta_2\sqrt{\theta_2}} = \frac{w_f}{\delta_2\sqrt{\theta_2}}\left[\left(\frac{\varepsilon_{w_f}}{w_f}\right)^2 + \left(\frac{\varepsilon_{P_2}}{P_2}\right)^2 + \frac{1}{4}\left(\frac{\varepsilon_{T_2}}{T_2}\right)^2\right] \tag{C8}$$

The last term of equation (C4) is zero because both P_1 and P_2 have the same common error. Also, both equations (C2) and (C3) yield the same value for efficiency error.

REFERENCES

1. Armentrout, E. C.; and Kicks, J. C.: Pressure Instrumentation for Gas Turbine Engines - A Review of Measurement Technology. NASA TM-73864, 1978.

2. Fleeger, D. W.; and Seyb, N. J.: Aerodynamic Measurements in Turbomachines. Modern Methods of Testing Rotating Components of Turbomachines (Instrumentation), M. Pianko, ed., AGARD-AG-207, 1975, pp. 79-121.

3. de Bogdan, C. E.; Moss, J. E., Jr.; and Braithwaite, W. M.: Internal Flow Characteristics of a Multistage Compressor with Inlet Pressure Distortion. NASA TM X-3446, 1977.

4. Lubomski, J. F.: Characteristics of Aeroelastic Instabilities in Turbomachinery - NASA Full Scale Engine Test Results. NASA TM-79085, 1979.

5. Lubomski, J. F.: Experimental Evaluation of the Effect of Inlet Distortion on Compressor Blade Vibrations. NASA TM-79066, 1979.

6. Bobula, G. A.; and Burkardt, L. A.: Effects of Steady-State Pressure Distortion on the Stall Margin of a J85-21 Turbojet Engine. AVRADCOM TR 79-12, NASA TM-79123, 1979.

7. Central Automatic Data Processing System. NACA TN-4212, 1958.

8. Glawe, G. E.; Hollanda, R.; and Krause, L. N.: Recovery and Radiation Corrections and Time Constants of Several Sizes of Shielded and Unshielded Thermocouple Probes for Measuring Gas Temperature. NASA TP-1099, 1978.

9. Keenan, J. H.; and Kaye, J.: Gas Tables. John Wiley & Sons, Inc., 1948.

10. Dean, R. C., Jr.: Aerodynamic Measurements. Massachusetts Institute of Technology Press, 1953.

11. Gettleman, C. C.; and Krause, L. N.: Considerations Entering into the Selection of Probes for Pressure Measurement in Jet Engines. ISA Paper 52-12-1, Sept. 1952.

12. Krause, L. N.; and Gettleman, C. C.: Effect of Interaction Among Probes, Supports, Duct Walls and Jet Boundaries on Pressure Measurements in Ducts and Jets. ISA Paper 52-12-2, Sept. 1952.

13. Kline, S. J.; and McClintock, F. A.: Describing Uncertainties in Single-Sample Experiments. Mech. Eng., vol. 75, no. 1, Jan. 1953, pp. 3-8.

14. Thrasher, L. W.; and Binder, R. C.: A Practical Application of Uncertainty Calculations to Measured Data. Trans. ASME, vol. 79, Feb. 1957, pp. 373-376.

15. Abernethy, R. B.; et al.: Handbook: Uncertainty in Gas Turbine Measurements. ARO-ETF-TR-72-60, Aro, Inc., 1973. (AEDC-TR-73-5, AD-755356)

16. Ascough, J. C.: The Accuracy of Thrust in Flight Derived from Engine Calibrations in an Altitude Test Facility. ICAS Paper 76-30, Oct. 1976.

TABLE I. - STATOR-PASSAGE BLOCKAGE RESULTING FROM INTERNAL INSTRUMENTATION

Stage	Average blockage, percent		Blockage range, percent	
	Pressure	Temperature	Pressure	Temperature
1	2.5	2.5	2-3.5	2-3.5
2	3.5	3.5	3-4.5	3-4.5
3	4.5	4.5	3.5-5.5	3.5-5.5
4	19	18	16-21	13-23
5	17	18	16-21	14-22
6	16	22	13-21	17-27
7	18	18	13-22	17-19
8	12	17	12-13	16-17
9	14	13	10-17	12-14

TABLE II. - PERFORMANCE SUMMARY AT ZERO NPI AND 1.0 RNI

Parameter	Value	Systematic uncertainty	Data scatter
Nozzle position indicator, NPI, percent	0	±0.3	[a]±0.3
Pressure ratio, P_3/P_2	8.30	±0.02	±0.02
Compressor adiabatic efficiency, η_c, percent			
Without interstage rakes	81.6	±0.6	±0.4
With interstage rakes	81.3	±0.6	±0.4
Corrected airflow, $w_a\sqrt{\theta_2}/\delta_2$, kg/sec (lbm/sec)	24.05 (53.0)	±0.15 (±0.3)	±0.15 (±0.3)
Corrected speed, $N/\sqrt{\theta_2}$, percent	100.0	±0.1	±0.25
Corrected turbine exit temperature, T_5/θ_2, K ($^\circ$R)	1000 (1800)	[b]±4 (±7)	±4 (±7)
Corrected fuel flow, $w_f/\delta_2\sqrt{\theta_2}$, g/sec (lbm/hr)	448 (3560)	±2 (±15)	±4 (±30)

[a]Throttle movement is taken into account in determining this value.
[b]Error from profile distribution is not included.

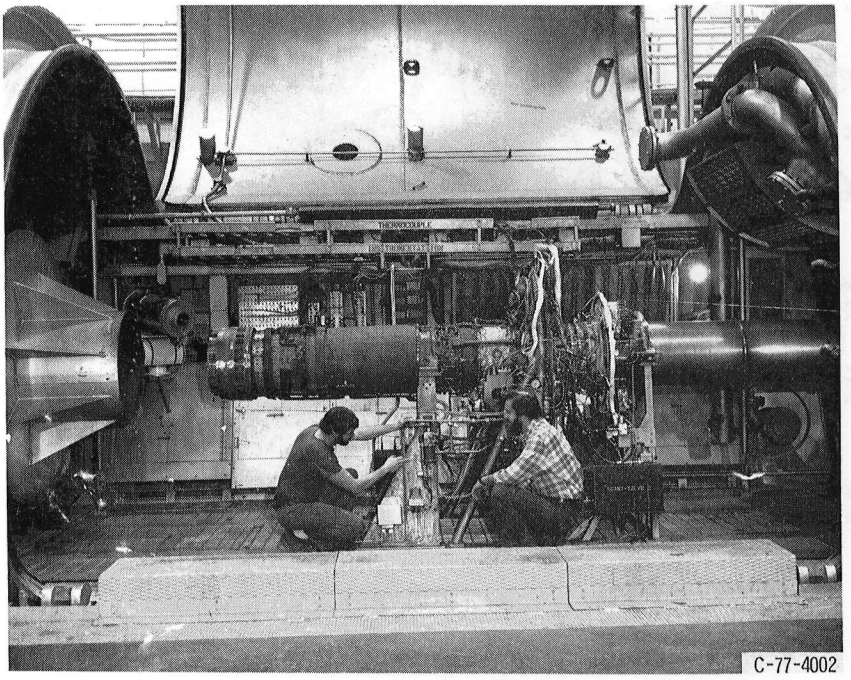

Figure 1. - J85-21 engine installation in altitude test chamber.

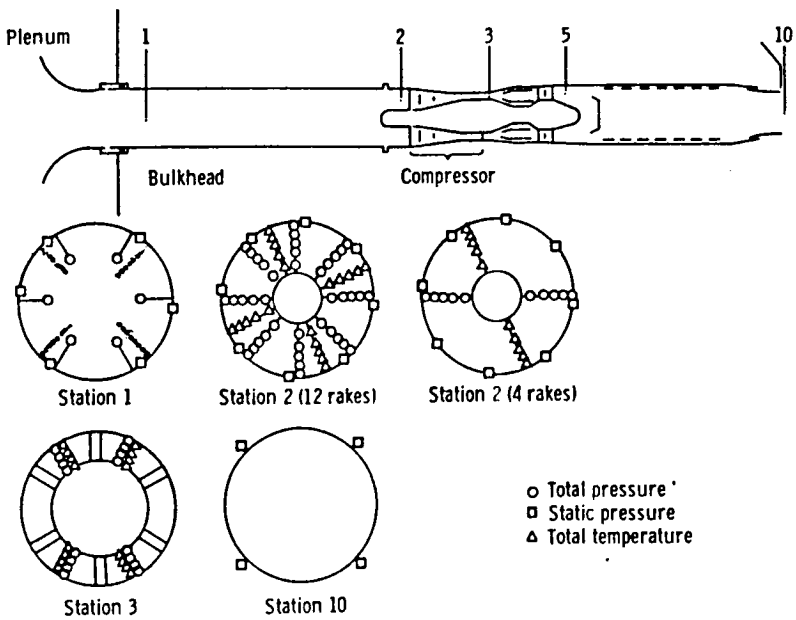

Figure 2. - Instrumentation layout for J85-21 engine, compressor interstage instrumentation not shown. (Stations viewed looking upstream.)

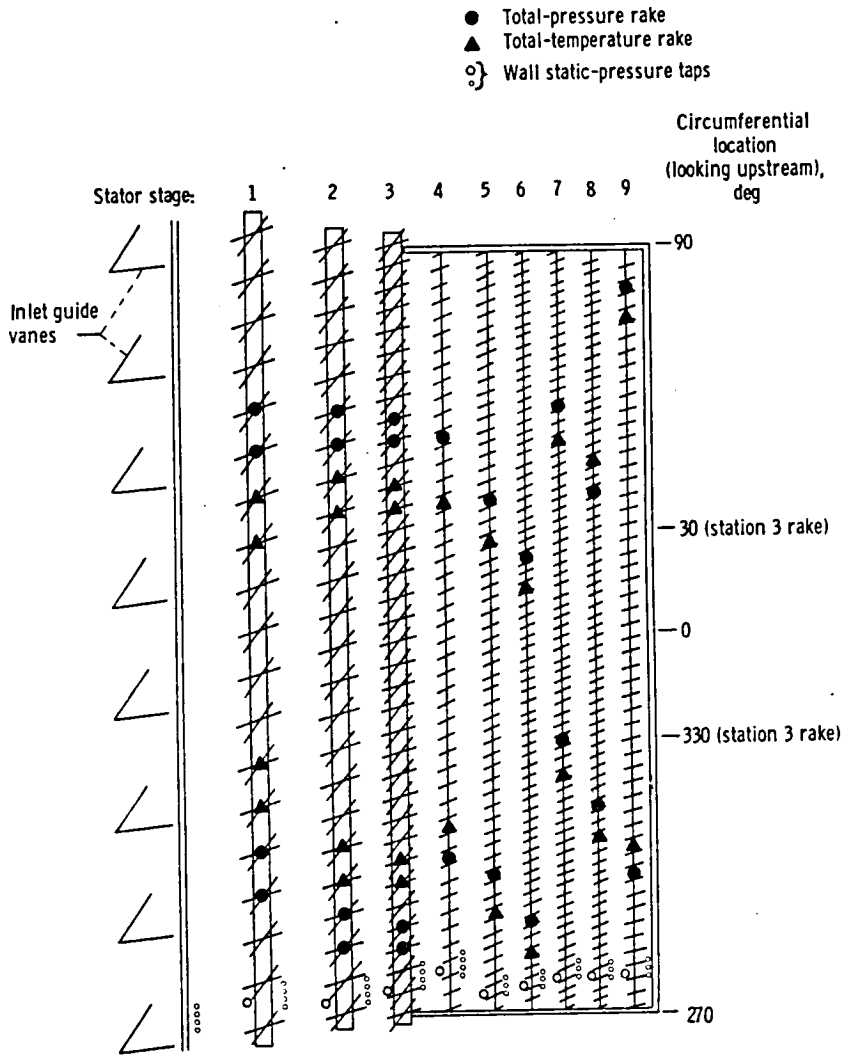

(a) Twenty-four vanes and 24 interstage rakes.

Figure 3. - Interstage instrumentation locations shown on unwrapped upper compressor case.

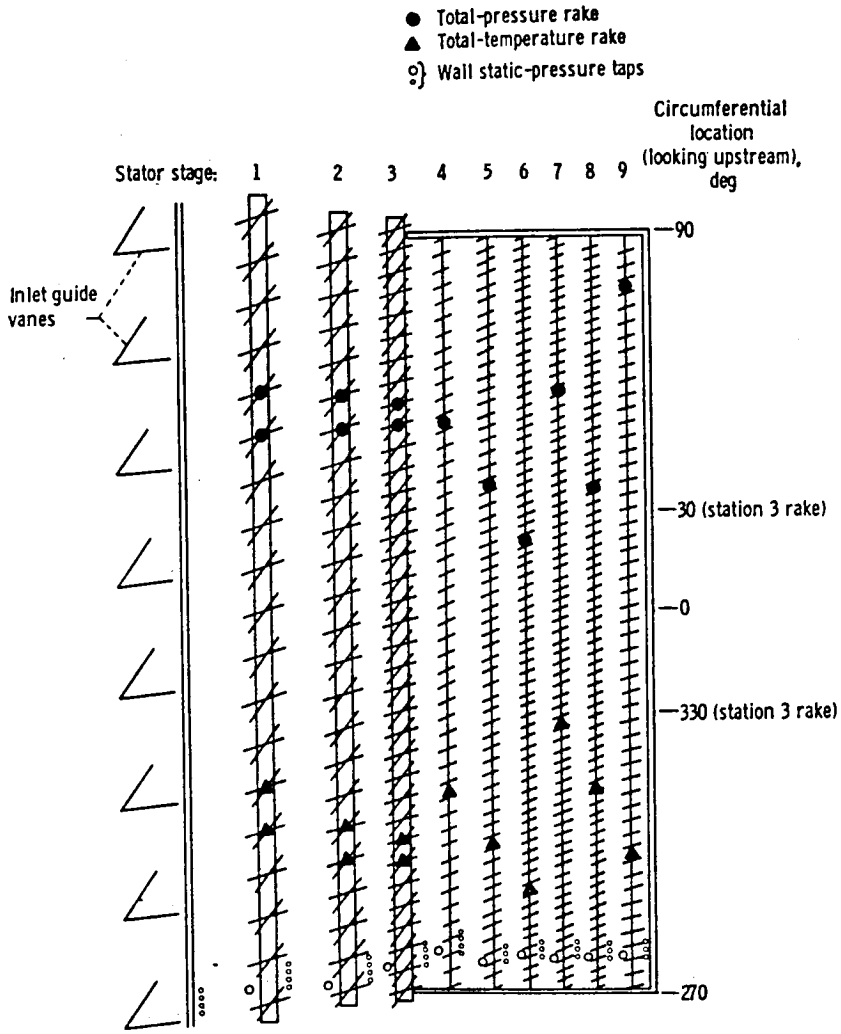

(b) Twelve vanes and 12 interstage rakes.

Figure 3. - Concluded.

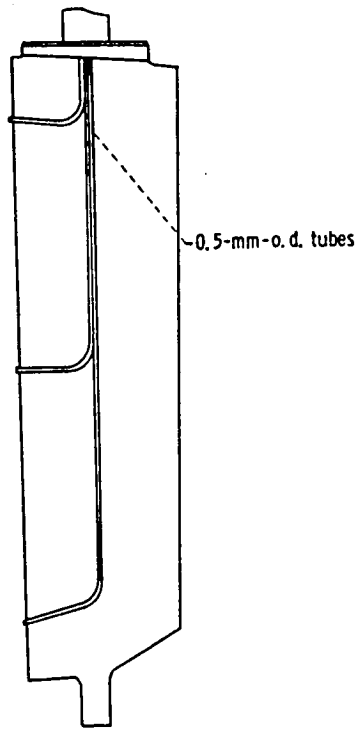

Figure 4. - Typical vane instrumentation.

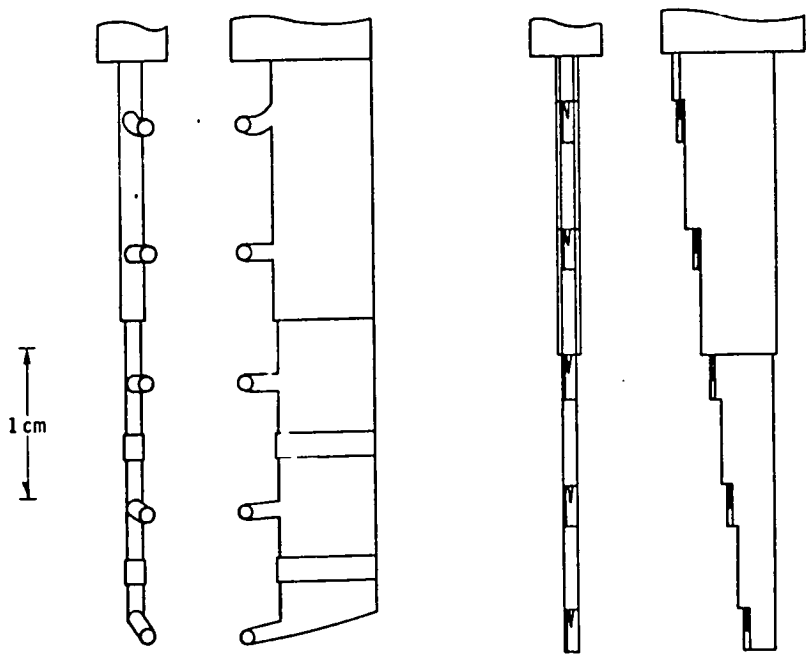

(a) Pressure.

(b) Temperature.

Figure 5. - Typical interstage rake designs.

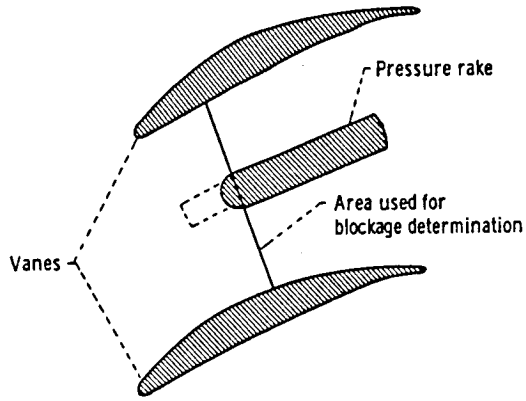

Figure 6. - Typical stator passage, pressure rake, and flow area used for blockage determination. Blockage, 19 percent.

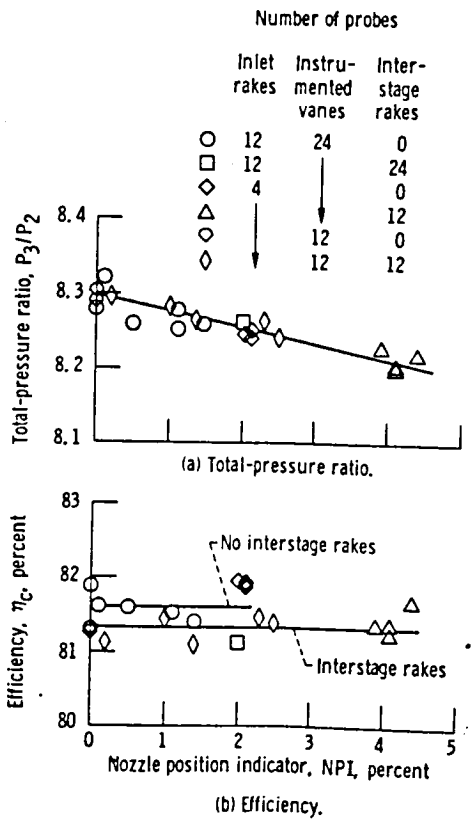

Figure 7. - Variation of compressor pressure ratio and efficiency at 1.0-Reynolds-number-index inlet conditions.

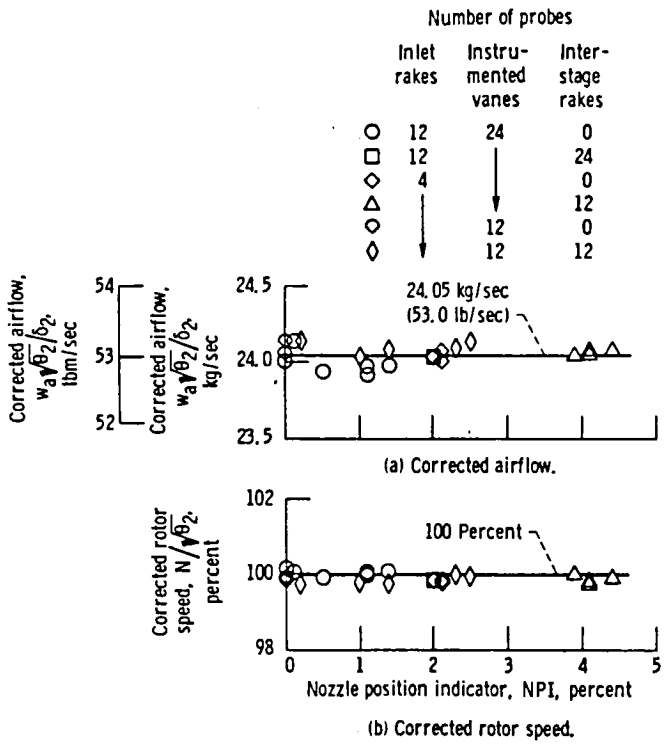

Figure 8. - Variation of corrected airflow and corrected rotor speed at 1.0-Reynolds-number-index inlet conditions.

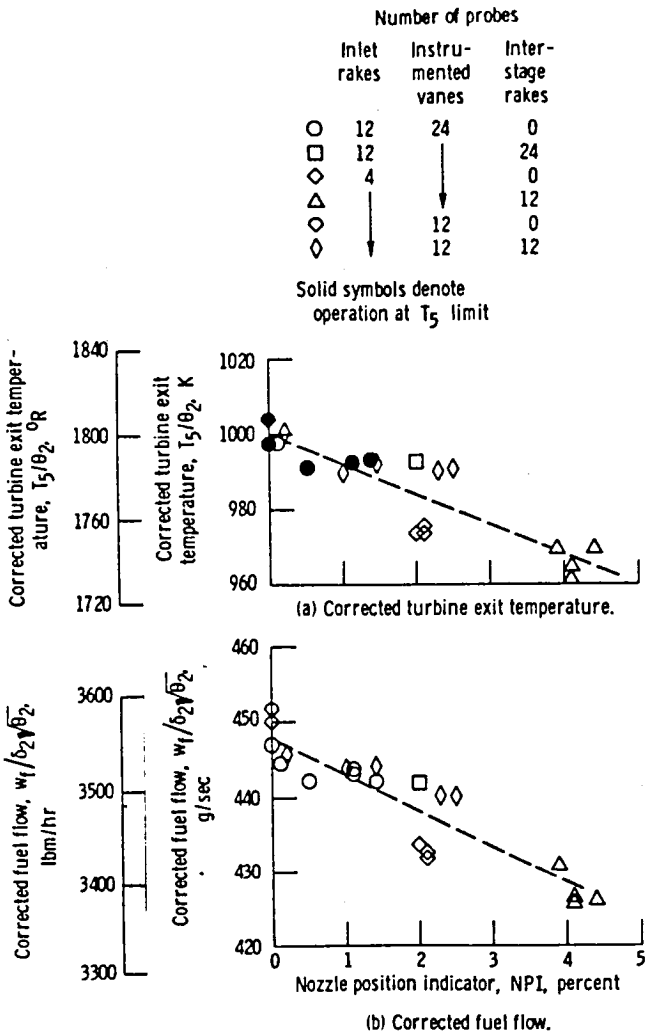

Figure 9. - Variation of corrected turbine exit temperature and corrected fuel flow at 1.0-Reynolds-number-index inlet conditions.

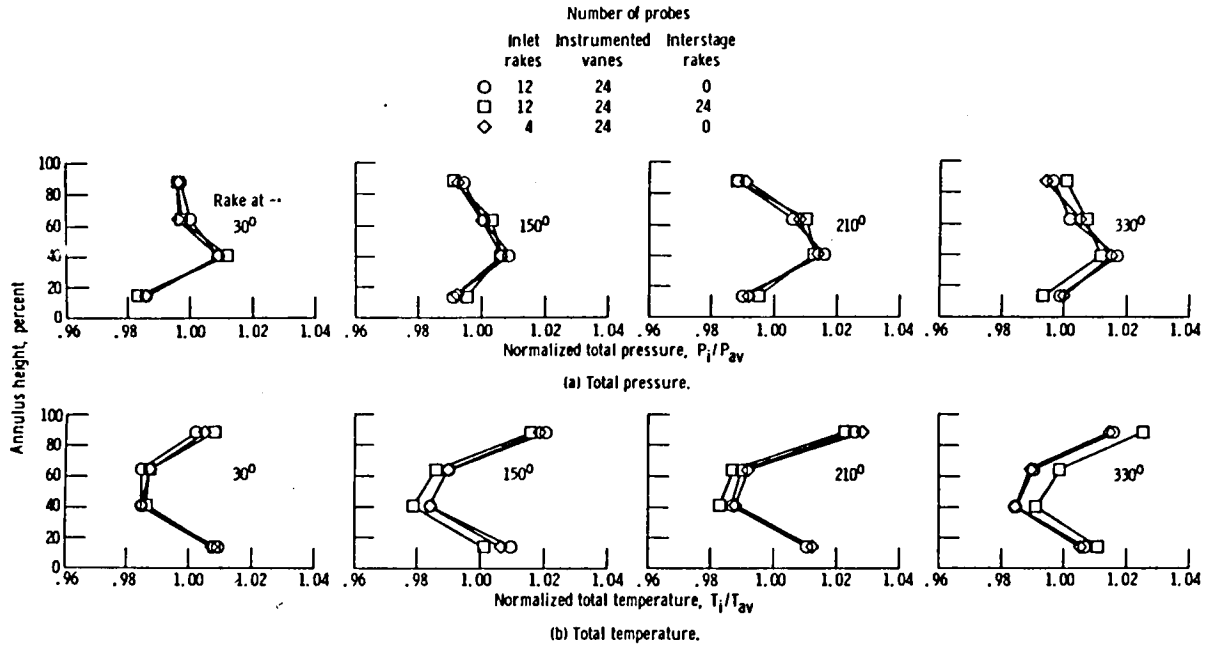

Figure 10. - Variation of compressor exit total pressure and temperature at 1.0-Reynolds-number-index inlet conditions - inlet and interstage rake configurations compared.

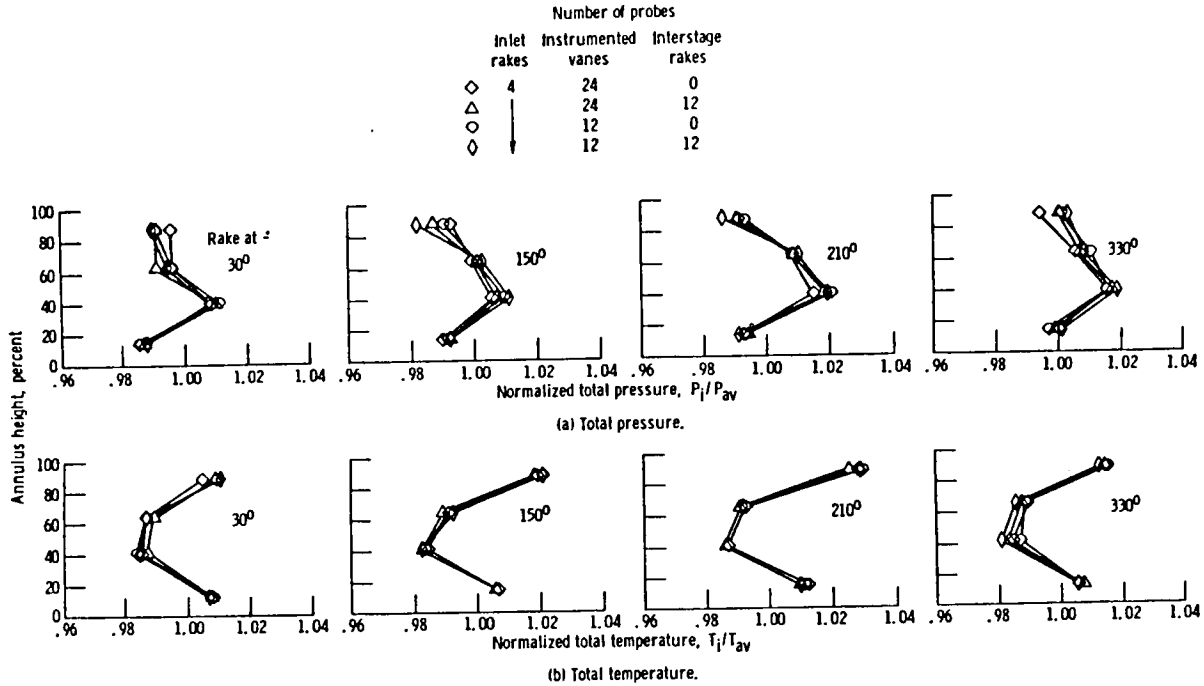

Figure 11. - Variation of compressor exit total pressure and temperature at 1.0-Reynolds-number-index inlet conditions - instrumented vane and interstage rake configurations compared.

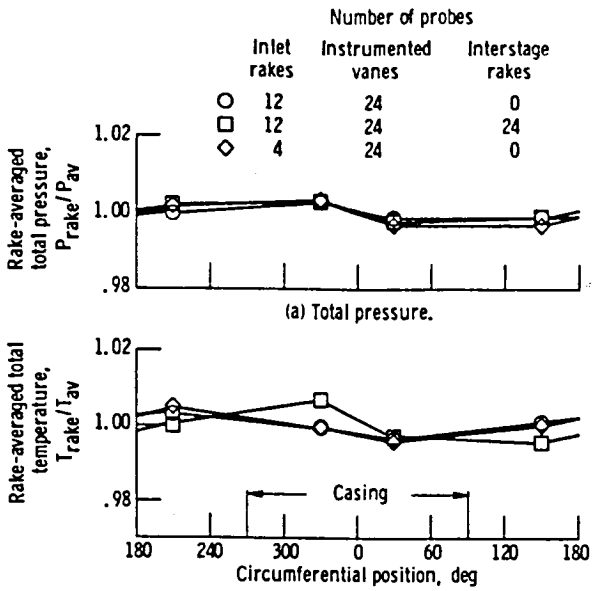

Figure 12. - Circumferential variation of rake-averaged compressor exit total pressure and temperature at 1.0-Reynolds-number-index inlet conditions - inlet and interstage rake configurations compared.

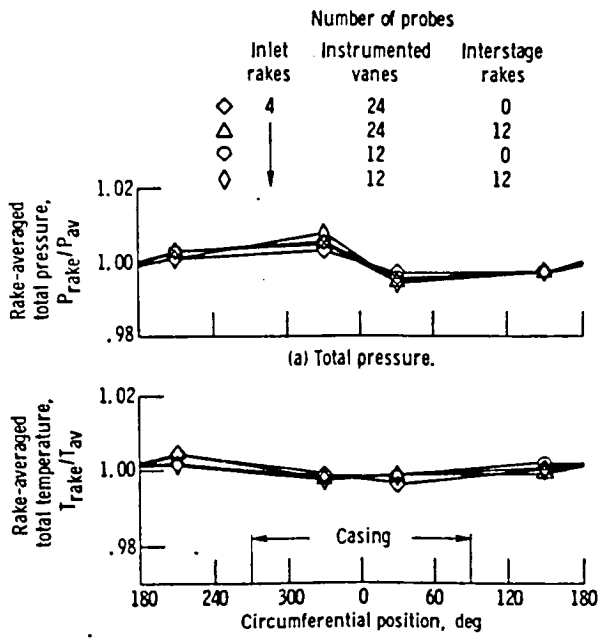

Figure 13. - Circumferential variation of rake-averaged compressor exit total pressure and temperature at 1.0-Reynolds-number-index inlet conditions - instrumented vane and interstage rake configurations compared.

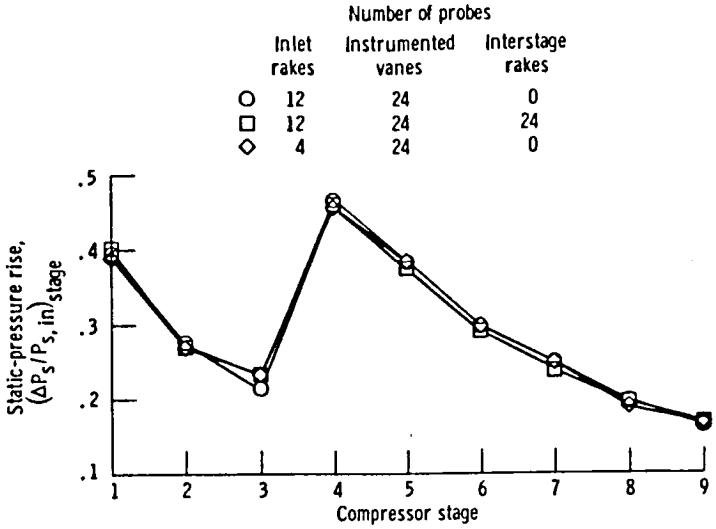

Figure 14. - Compressor stage static-pressure rise at 1.0-Reynolds-number-index inlet conditions - inlet and interstage rake configurations compared.

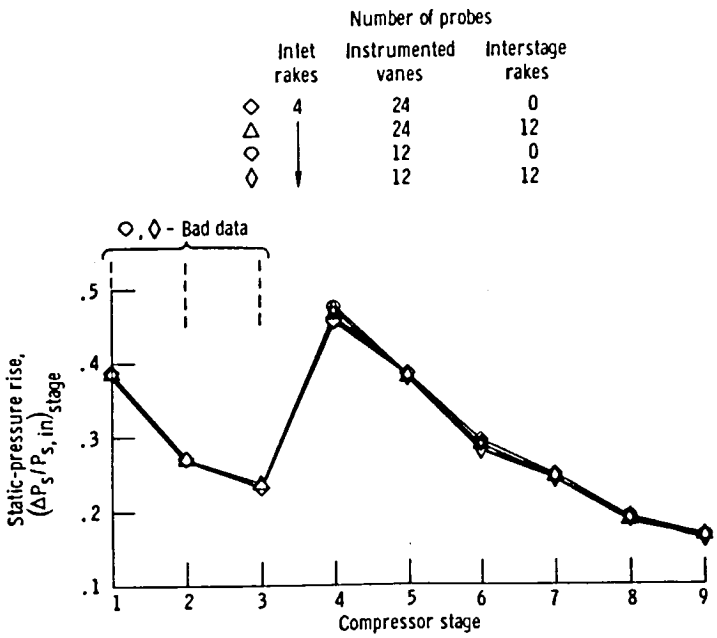

Figure 15. - Compressor stage static-pressure rise at 1.0-Reynolds-number-index inlet conditions - instrumented vane and interstage rake configurations compared.

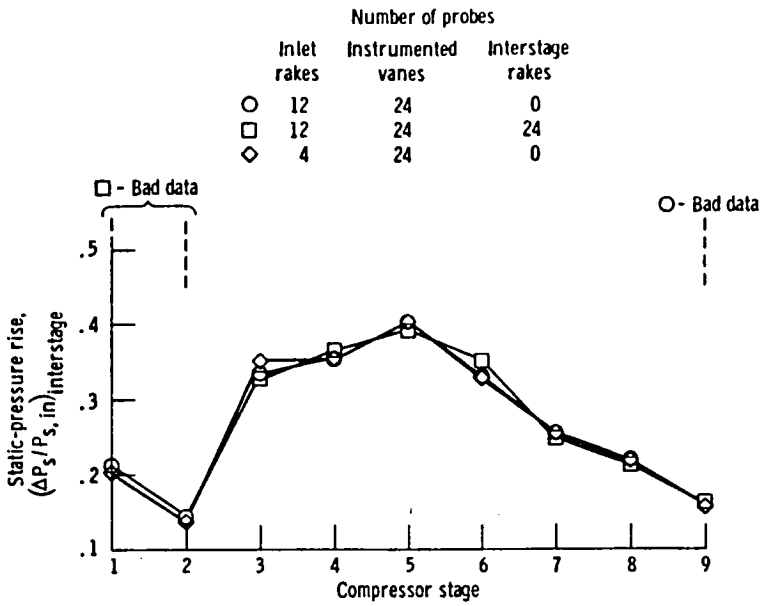

Figure 16. - Compressor interstage static-pressure rise at 1.0-Reynolds-number-index inlet conditions - inlet and interstage rake configurations compared.

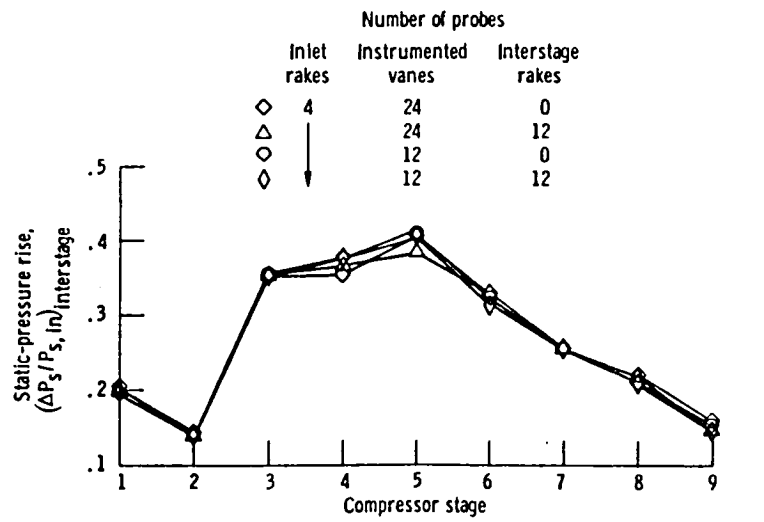

Figure 17. - Compressor interstage static-pressure rise at 1.0-Reynolds-number-index inlet conditions - instrumented vane and interstage rake configurations compared.

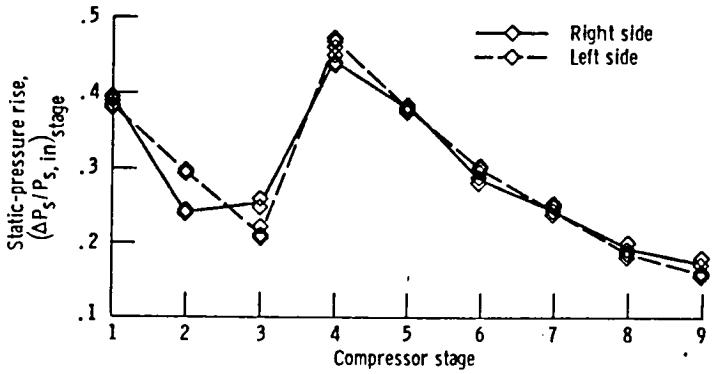

Figure 18. - Right- and left-side compressor stage static-pressure rise for 4 inlet, 24 vane, and 0 interstage rake instrumentation, at 1.0-Reynolds-number-index inlet conditions.

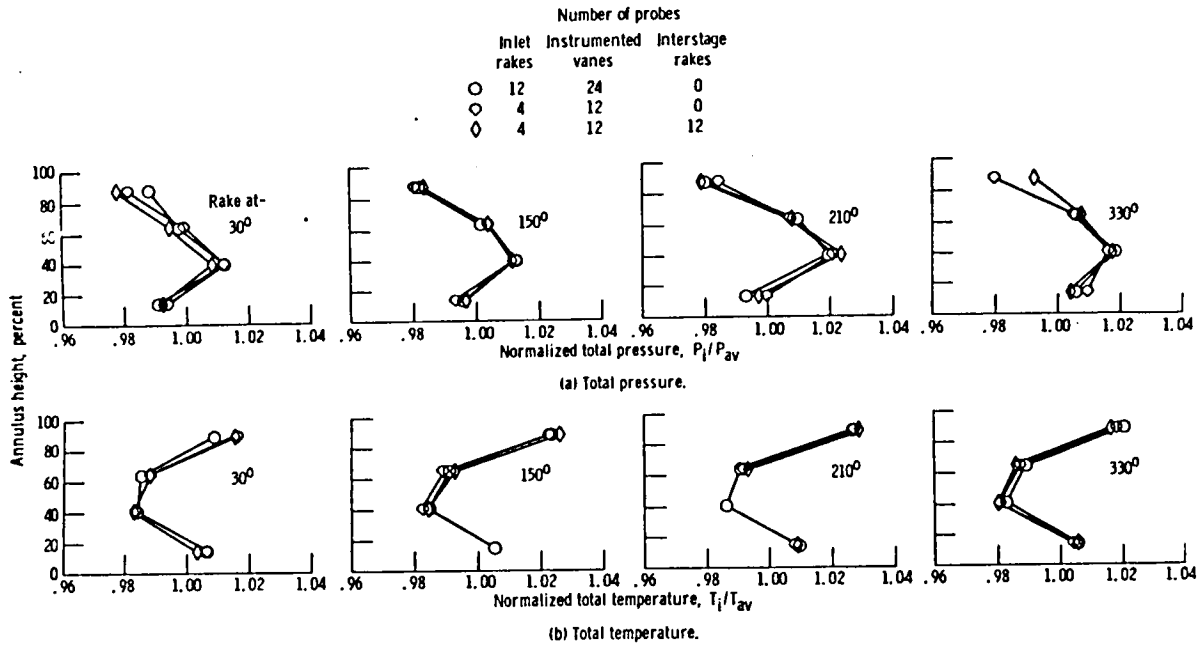

(a) Total pressure.

(b) Total temperature.

Figure 19. - Variation of compressor exit (station 3) total pressure and total temperature at 1.69-Reynolds-number-index inlet conditions.

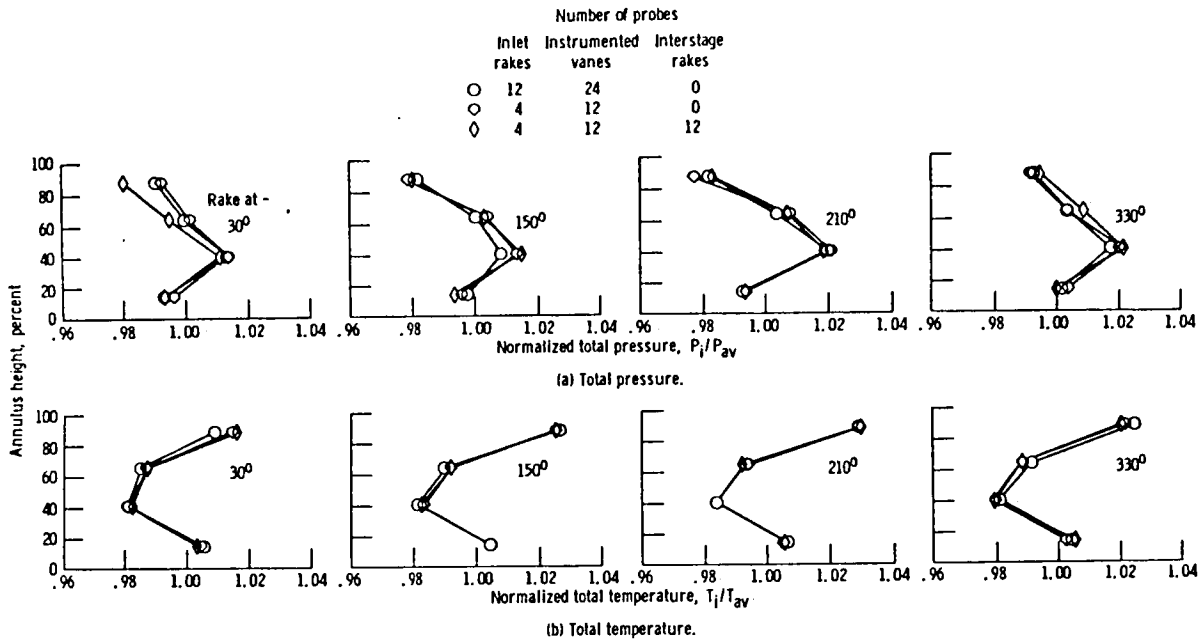

Figure 20. - Variation of compressor exit (station 3) total pressure and total temperature at 1.95-Reynolds-number-index inlet conditions.

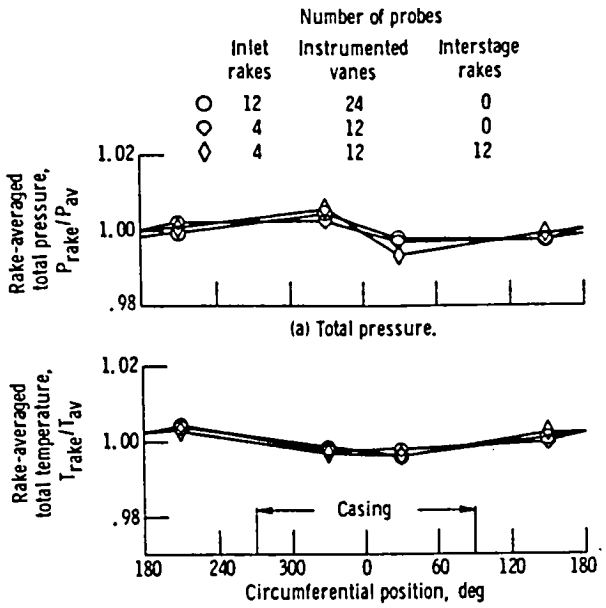

Figure 21. - Circumferential variation of rake-averaged compressor exit (station 3) total pressure and total temperature at 1.69-Reynolds-number-index inlet conditions.

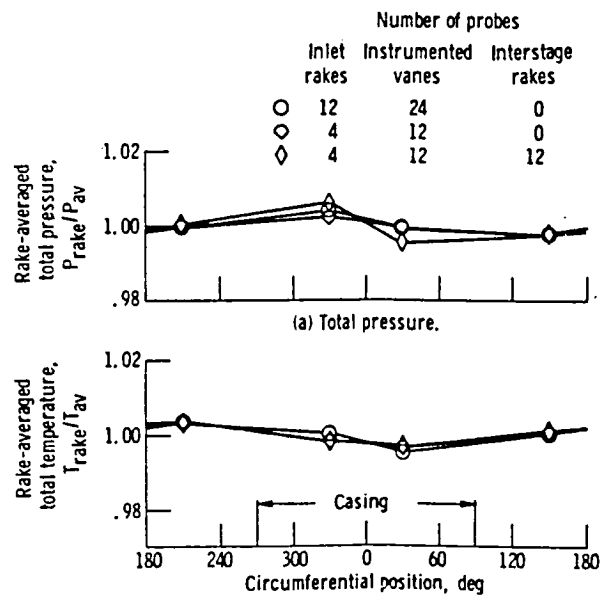

Figure 22. - Circumferential variation of rake-averaged compressor exit (station 3) total pressure and total temperature at 1.95-Reynolds-number-index inlet conditions.

	Reynolds number index, RNI_1	Mach number, M_1	Corrected airflow, $\frac{w_a\sqrt{\theta_1}}{\delta_1}$
○	1.00	0.35	22.5 (49.5)
□	.69	.35	22.4 (49.2)
◇	.51	.34	21.9 (48.2)
△	.38	.32	21.1 (46.4)

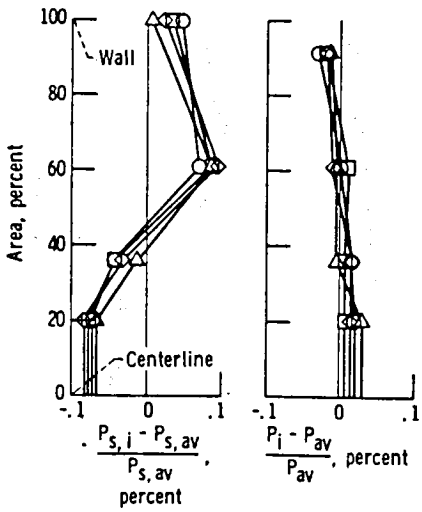

(a) Static pressure. (b) Total pressure.

Figure 23. - Radial variation of static and total pressure at airflow station (station 1).

1. Report No.	2. Government Accession No.	3. Recipient's Catalog No.
NASA TM-81451		

4. Title and Subtitle	5. Report Date
STEADY-STATE PERFORMANCE OF A J85-21 COMPRESSOR AT 100 PERCENT OF DESIGN SPEED WITH AND WITHOUT INTERSTAGE RAKE BLOCKAGE	March 1980
	6. Performing Organization Code
7. Author(s)	8. Performing Organization Report No.
Roger A. Werner	E-377
	10. Work Unit No.
9. Performing Organization Name and Address	
National Aeronautics and Space Administration Lewis Research Center Cleveland, Ohio 44135	11. Contract or Grant No.
	13. Type of Report and Period Covered
12. Sponsoring Agency Name and Address	Technical Memorandum
National Aeronautics and Space Administration Washington, D.C. 20546	14. Sponsoring Agency Code

15. Supplementary Notes

16. Abstract

Internal compressor instrumentation blockage effects on steady-state J85-21 compressor performance at 100 percent of design speed are determined. The blockage was generated by instrumented vanes for the first three compressor stages and by removable rakes for stages 4 to 9. Individual flow-passage blockages ranged up to 4.5 percent with the instrumented vanes and up to 22 percent with the removable interstage rakes. At a Reynolds number index of 1.0, pressure ratio and airflow remained unchanged with insertion of the interstage rakes, but efficiency dropped 0.3 percentage point. Compressor exit profiles, compressor stage static-pressure-rise coefficients, turbine exit temperature, and fuel flow are also presented.

17. Key Words (Suggested by Author(s))	18. Distribution Statement
Compressor performance Instrumentation blockage Steady state Experimental Turbojet	Unclassified - unlimited STAR Category 07

19. Security Classif. (of this report)	20. Security Classif. (of this page)	21. No. of Pages	22. Price*
Unclassified	Unclassified		

* For sale by the National Technical Information Service, Springfield, Virginia 22161

National Aeronautics and
Space Administration

Washington, D.C.
20546

Official Business
Penalty for Private Use, $300

SPECIAL FOURTH CLASS MAIL
BOOK

Postage and Fees Paid
National Aeronautics and
Space Administration
NASA-451

NASA

POSTMASTER: If Undeliverable (Section 158
Postal Manual) Do Not Return